Nanoscale



PAPER View Article Online
View Journal | View Issue



Cite this: Nanoscale, 2023, 15, 5011

Unveiling growth and dynamics of liposomes by graphene liquid cell-transmission electron microscopy†

Liposome is a model system for biotechnological and biomedical purposes spanning from targeted drug delivery to modern vaccine research. Yet, the growth mechanism of liposomes is largely unknown. In this work, the formation and evolution of phosphatidylcholine-based liposomes are studied in real-time by graphene liquid cell-transmission electron microscopy (GLC-TEM). We reveal important steps in the growth, fusion and denaturation of phosphatidylcholine (PC) liposomes. We show that initially complex lipid aggregates resembling micelles start to form. These aggregates randomly merge while capturing water and forming small proto-liposomes. The nanoscopic containers continue sucking water until their membrane becomes convex and free of redundant phospholipids, giving stabilized PC liposomes of different sizes. In the initial stage, proto-liposomes grow at a rate of 10-15 nm s⁻¹, which is followed by their growth rate of 2-5 nm s⁻¹, limited by the lipid availability in the solution. Molecular dynamics (MD) simulations are used to understand the structure of micellar clusters, their evolution, and merging. The liposomes are also found to fuse through lipid bilayers docking followed by the formation of a hemifusion diaphragm and fusion pore opening. The liposomes denaturation can be described by initial structural destabilization and deformation of the membrane followed by the leakage of the encapsulated liquid. This study offers new insights on the formation and growth of lipid-based molecular assemblies which is applicable to a wide range of amphiphilic molecules.

Received 2nd November 2022, Accepted 10th February 2023 DOI: 10.1039/d2nr06147c

rsc.li/nanoscale

Introduction

Liposomes, vesicles formed by self-assembly of lipid bilayers, have a similar structure to biological cell membranes, making them a model system for biotechnological and biomedical purposes. Simplicity of synthesis, tunable physicochemical properties, biodegradability, biocompatibility, and ability to encapsulate and release different substances make these lipid vesicles attractive drug carriers. Development of lipid-based formulations to enhance recombinant vaccine antigens immunogenicity is of high interest to modern vaccine research, for example, COVID-19 vaccine. Liposomes are also used as micro/nanoreactor to synthesize nanoparticles and have potential for numerous other applications. Liposomes are thermodynamically unstable and tend to fuse, aggregate, and

denature, limiting their applications. 18-20 Therefore, acquiring

a deep understanding of liposomes in native and hydrated

an emerging technique for observing evolution and dynamics of hard and soft matter in liquid. 21-23 Unlike commonly used solid-state TEM techniques such as staining,24 freeze-fracture,25 and cryogenic TEM (cryo-TEM), 25,26 the in situ LC-TEM offers an indispensable platform to study molecular structures in hydrated environment.^{3,8,21-23,27} However, low atomic number, increased electron scattering due to the presence of thick solvent and silicon nitride (SiN_x) membranes, and electron radiation-induced damage are among many challenges to limit the spatial imaging and chemical resolution in studying soft/ organic materials by LC-TEM techniques that utilize SiN_x membranes. 9,21,23 For instance, SiN_x-based LC-TEM was used to study the formation and evolution of the liposomes due to poor spatial resolution resulting from two 50 nm thick SiN_x membranes and 150 nm thick solvent (water) layer prevented the nanoscale observation of formation and growth of liposomes.³

environment can expand our knowledge about cell membranes behavior in aqueous environment such as endocytosis and exocytosis, engineering liposomes for targeted drug delivery, materials synthesis, and many others. Liquid cell-transmission electron microscopy (LC-TEM) is

^aMechanical and Industrial Engineering Department, University of Illinois at Chicago, Chicago, IL 60607, USA. E-mail: rsyassar@uic

^bDepartment of Chemistry, University of Illinois at Chicago, Chicago, IL 60607, USA ^cDepartment of Physics, Pharmaceutical Sciences, and Chemical Engineering, University of Illinois at Chicago, Chicago, USA

[†]Electronic supplementary information (ESI) available. See DOI: https://doi.org/ 10.1039/d2nr06147c

The emergence of graphene liquid cells (GLCs) where a submicrometer liquid is trapped between graphene sheets that are impermeable to small molecules has created new frontiers in the area of electron microscopy. 28-33 In general, GLC-TEM allows to enhance the signal-to-noise ratio and image resolution, mitigate solvent evaporation under the high vacuum environment of TEM, and minimize sample damage (e.g. charging, degradation, and ionization induced by electron beam radiation) during imaging. 21,23 Biomaterials are reported to show higher electron dose tolerance (approximately one order of magnitude) when imaged in GLC, compared to imaging in cryo-TEM. 34-38 Single molecule analysis of cell membrane proteins and dynamics of DNA molecules anchored gold nanoparticles are also studied in GLC. 29,33 In a recent study, Nagamanasa et al. used GLC-TEM to visualize absorption behavior and conformational changes of individual molecules of poly(ethylene oxide) and polystyrene sulfonate in aqueous solution.²³

Herein, we visualized the evolution of the phosphatidylcholine (PC) liposomes formed through self-assembly of phosphatidylcholine model lipids by GLC-TEM in real-time. Our findings show that the formation of PC liposomes can occur in three distinct stages: (i) fast initial growth rate (10-15 nm s⁻¹) corresponding to the formation of small liposomes from micelle-like structures and their aggregation; (ii) slow growth rate (2-5 nm s⁻¹) during the lipids diffusion and liposome growth; and (iii) Low or no growth rate indicating the size stability of mature liposomes. PC liposomes are also found to fuse through lipid bilayers docking followed by the formation of a hemifusion diaphragm and the fusion pore opening. Furthermore, liposomal denaturation is monitored which include initial structural destabilization and deformation of the lipid bilayer followed by rupture and leakage of the encapsulated liquid and complete disintegration of the membrane.

Experimental procedure

Materials

L-α-Phosphatidylcholine (PC) from egg (99% lecithin, [(2R)-3hexadecanoyloxy-2-[(Z)-octadec-9-enoyl] oxypropyl] 2-(trimethylazaniumyl)ethyl phosphate, Product no# 840051, Avanti Lipids), chloroform (Sigma-Aldrich), anhydrous ethanol (EtOH, anhydrous, ≥99.5%, Sigma-Aldrich), methanol (MeOH, Sigma-Aldrich), sodium persulfate (Na₂S₂O₈, >98%, Fisher), water for HPLC (Sigma-Aldrich), carbon-coated gold TEM grids (Electron Microscopy Sciences), graphene coated copper foil (Electron Microscopy Sciences) are used as received.

Protocol for synthesis of liposome

PC (33 mg, mmol) and cholesterol (7 mg, mmol) are dissolved in chloroform (3 ml). Solvent is removed under reduced pressure using a rotary evaporator at 40 °C, leaving a thin film of dry lipid on wall of the flask. The evaporation is continued for at least 1 h to ensure complete removal of the organic solvent traces. Afterwards, the obtained film is hydrated by

adding 20 ml PBS buffer solution (pH 7.2, MgCl₂, CaCl₂) and the mixture is stirred or vortexed until a homogenous suspension is obtained. The suspension is subjected to sonication (500 W, 30% sonication strength with the sequence of 1 s sonication and 1 s rest for 5 min to decrease the size of forming liposomes. To better understand the effects of salts in PBS on PC liposomes, a similar protocol is performed except ultrapure water (no salt) is used instead of the PBS solution. For the PC solution with no cholesterol and salt, a similar protocol is performed in the absence of cholesterol and ultrapure water (no salt) is used instead of the PBS solution.

Protocol for preparation of graphene-coated gold TEM grids

To prepare graphene-coated Au TEM grids, a general protocol is performed as follows: 200 or 300 mesh carbon-coated Au grids from carbon-coated side are gently placed onto a small piece of a smooth graphene-on-Cu foil (Fig. S1a†). Having a smooth surface ensure a good contact between the graphene layer and carbon layer of the Au grid. Then, a few drops of isopropanol are poured onto the grids or foil and allowed to dry for approximately 2-3 hours (Fig. S1b†). Isopropanol ensures a good contact between the carbon film on the Au grids and the coating graphene layer. Then, the Cu foil is etched by gently laying down graphene-on-Cu piece on the Na₂S₂O₈ etching solution (made of 1 g of Na₂S₂O₈ in 10 ml ultrapure water) and keep it for approximately 20 hours (Fig. S1c and S1d†). At the last step, remove the floating graphene-coated Au grids and rinse with water (in a Petri dish) for at least three times to ensure full removal of the etched Cu (Fig. S1e†). Afterwards, the graphene-coated Au grids are dried under a lamp or at ambient temperature (Fig. S1f†).

Graphene liquid cell-transmission electron microscopy (GLC-TEM)

Graphene-liquid cell (GLC) are formed by putting a small droplet (~0.2 μl) of the PC lipid aqueous solution onto a graphene-coated TEM grid and the second graphene-coated TEM grid is gently located on top of the bottom grid. Excess solution is removed by blotting the edge of the grid with filter paper, followed by laying a top graphene chip, or cover chip, onto the bottom chip, leading to producing the creases in the top graphene sheet and trapping the liquid. The graphene sheets provide the required mechanical integrity for the liquid pockets. The GLC-TEM imaging is performed on a JEM-ARM200 (JEOL, Ltd) operated at 200 keV and micrographs were recorded on 2K × 2K Orius SC200 CCD camera (Gatan Inc.).

Dry-state transmission electron microscopy (TEM)

A small aliquot $(1 \mu l)$ of the sample is manually pipetted onto a carbon-coated Cu TEM grid. Excess solution is removed by blotting the edge of the grid with filter paper, and then the sample-loaded grid was dried by evaporation at ambient temperature. The TEM imaging is performed on a JEM-ARM200 (JEOL, Ltd) operated at 200 keV and micrographs were recorded on 2K × 2K Orius SC200 CCD camera (Gatan Inc.).

Nanoscale Paper

Image analysis

In situ TEM videos captured at 6 frame per seconds were analyzed using ImageJ. The size of liposomes during formation and growth are measured for all the frames with 0.16 s time interval. The resolution of image is 3.16 pixels per nm. For better visualization of contrast change during the process, a lookup table (Mpl-viridis LUT) is applied to the original black and white images where each grayscale intensity is assigned a corresponding RGB value representing a particular color. In Mpl-viridis LUT applied images, yellow and dark purple colors represent the white and black with highest and lowest intensity in gray scale values respectively.

Molecular dynamics (MD) simulations

MD simulations were performed with the NAMD (Nanoscale Molecular Dynamics) software package³⁹ in an NPT ensemble at T=298 K, using the Langevin dynamics with a damping constant of $\gamma_{\rm Lang}=0.1~{\rm ps}^{-1}$ and a time step of 1 fs. The CHARMM (Chemistry at Harvard Macromolecular Mechanics) general force field^{40,41} was implemented for the bond, angle, and dihedral parameters of ions, water, PC, and cholesterol molecules. Nonbonding interactions between these molecules, such as a van der Waals (vdW) attraction and a steric repulsion, were described by the Lennard-Jones (LJ) potential,

$$U_{\mathrm{LJ}}(r) = arepsilon \left[\left(rac{r_{\mathrm{min}}}{r}
ight)^{12} - 2 \left(rac{r_{\mathrm{min}}}{r}
ight)^{6}
ight],$$

where ε is the minimum (negative) energy of the coupling and r_{\min} is a distance where $U_{\rm LJ}(r_{\min})$ has a local minimum, both of which are provided by the CHARMM force field. The r^{-12} and r^{-6} terms represent an atomic repulsion due to overlapping electron orbitals and the vdW attractive coupling, respectively. The LJ potential implemented in NAMD has a typical cutoff distance of 1 nm. The electrostatic coupling between ions and partially charged atoms, which also belongs to nonbonding interactions, has a cutoff similar to that of the LJ potential, but its long-range part is calculated by the particle mesh Ewald (PME) method⁴² in the presence of periodic boundary conditions. The systems were run in a 19 nm periodic water box comprising randomly oriented PC molecules and ions with and without the presence of 25 mol% of cholesterol.

Results and discussion

Behavior of liposomes in a dynamic environment including their formation and growth, fusion and denaturation can be visualized in real-time using LC-TEM. ^{2,3} *In situ* study of the growth of liposomes by self-assembly of lipids in aqueous environment enables us to acquire a deeper understanding of the intermediate pathways for liposome formation. Thus, the goal is to monitor liposomes formed by self-assembly of phospholipids in real-time using GLC-TEM. Fig. 1 shows schematic illustration of the synthesis of PC liposome *via* self-assembly of the phospholipids in aqueous phase (Fig. 1a) and loading the liposomal solution into GLC for *in situ* study (Fig. 1b and

c). A detailed description of fabricating graphene-coated TEM grids and assembly of GLC is demonstrated in Fig. S1 and S2.†

Through in situ GLC-TEM visualization of the liposomal solution and their time-dependent growth behavior (Fig. 2a and b), we found that small PC liposomes initially start to form from lipid aggregates resembling micelle-like structures within the bulk solution. The original time-series of the TEM images is also shown in Fig. S3.† It appears that at the early stages and as molecular self-assembly becomes favored, the lipid-rich phase transforms into lipid aggregates or micelle-like structures (Fig. 2c and d). It suggests that the instability of phospholipids as amphiphilic molecules within the bulk polar medium led to the formation of lipids aggregates or micelle-like structures followed by their evolution to liposome (vesicle) as more stable assemblies. Therefore, vesiculation of micelles or transformation of small aggregates of amphiphilic lipid molecules into vesicle-like structures is a spontaneous process to minimize the surface tension energy due to exposure of the nonpolar hydrophobic tails of lipid molecules to polar water molecules. 43 In fact, there is a minimal interaction between the water molecules and hydrophobic tail of the phospholipids in a lipid bilayer. This is consistent with the previous reports suggesting the transition of micelle-like structures into liposomes shown by experimental studies (particle size measurements, electron microscopy) and theoretical studies (modelling and kinetics). 19,44-48

The exact mechanism by which the electron beam initiated the process is not clear, but we believe there are several possibilities: (1) one would be the existence of some isolated individual or small clusters of lipid molecules that did not have the opportunity to join the already formed liposome assemblies due to large diffusional distances. The input energy from electron beam can increase the dynamic of such individual or small lipid clusters, enabling them to come together and form the assemblies. One aspect that may influence the mobility of such lipid molecules can be local temperature rise. It is suggested that electron beam can increase the temperature of liquid solution. Fritsch et al.49 showed that constant irradiation of electron beam in liquid cell-TEM could significantly increase the local temperature (e.g., reaching up to 60 °C after 2 min). They have also reported that electron dose rate is proportional to the temperature of the liquid and temperature could increase up to 20 °C at electron flux of \sim 2 e A⁻² s⁻¹. Hsieh et al. 50 also reported (both experimentally and theoretically) that electron beam increases temperature up to 85 °C at high electron doses during in situ liquid cell-TEM study of ZnO nanocrystal formation. It is also suggested that the rate of phospholipids self-assembly increases by raising temperature due to changing the free energy and diffusion coefficients of phospholipids as well as lowering liquid viscosity. 18,51 It is also proposed that temperature raise in the liquid cell can significantly enhance the rate of radiolysis.^{52,53} However, one should note that there are conflicting reports on the temperature rise under electron beam. For instance, the work of Loh et al. 54 shows that the local change in temperature does not exceed 1-10 K. (2) The radiolysis products due to the interaction of electron beam with water molecules can locally

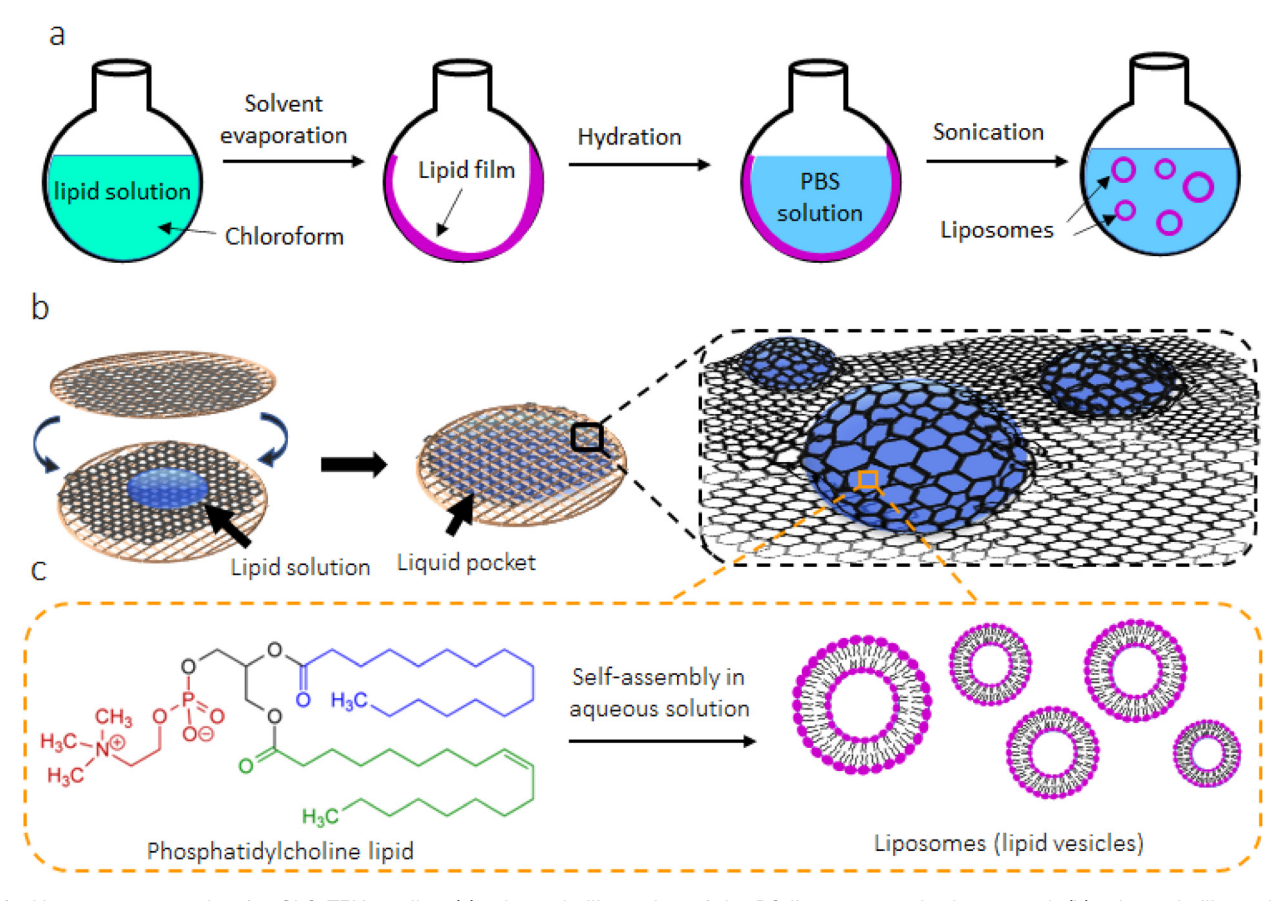


Fig. 1 Liposome preparation for GLC-TEM studies: (a) schematic illustration of the PC liposome synthesis protocol; (b) schematic illustration of encapsulation of the liposomal solution in liquid pockets of GLC; (c) the formation of phosphatidylcholine (PC) liposomes through self-assembly of phosphatidylcholine molecules.

dissolve some small or incomplete liposome assemblies and allow them to form again. This is understandable knowing that lipid assemblies are thermodynamically favored to form in water. In fact, electron beam-induced radiolysis is common in TEM imaging and water radiolysis byproducts (predominately e-aq, HO') can react with organic functional groups of liposomes and induce oxidative decomposition of lipids. 52,53,55 Similar to the chain scission in polymers, 56,57 electron beam radiation can lead to the oxidative degradation of lipids driven by loss of electrons, leading to instability and degradation of liposomes. The free lipids from the degraded liposomes can form new liposomes driven by thermodynamic stability of the lipids in a vesicle form. (3) The electron beam can also induce aggregation and clustering. 52,58,59 In fact, it was shown that stable colloidal suspensions aggregate during imaging by an electron microscope due to irradiation generated ions which increases the solution ionic strength and reduce Debye screening length and resulting repulsive force between particles. 58,59 Similarly, in our case, electron beam can lead to aggregation of lipid molecules, transforming them to micelle-like structures followed by liposomes.

One should note that the size of phosphatidylcholine is expected to be approximately 2 nm.60,61 The smallest structures captured in the data are about 15 nm, which is far larger than the micelle shows in the schematic in Fig. 2e. Note should be given that the schematic in Fig. 2e indeed represent aggregate or cluster of several lipids, which can take sizes up to tens of nanometers. In fact, these lipids are amphiphilic molecules, and similar to the other amphiphilic molecules such as block copolymers with hydrophilic-hydrophobic segments, they can form aggregates or micelle-like structures with a nonpolar or hydrophobic core (hydrocarbon chains) and polar or hydrophilic corona (phosphate/ammonium head group). In this manner, several lipid molecules form an aggregate or micelle-like structure to enhance the stability by minimizing the interaction between the nonpolar segment of the lipids and water medium. It is important to note that the formation of phospholipids-based micelle is reported in the literature, 19,44-48 yet, we have used the term "micelle-like structure" since we could not clearly indicate a distinct core and corona. However, the most thermodynamically stable form of the lipids is vesicle structure where there exists a minimal interaction between the hydrophobic segment and water medium. Therefore, we believe that these lipids aggregates or micelle-like structures act as intermediate to form the vesicle (liposome). Coexistence of such aggregates or micelle-like structures and liposomes is a good indicative of this transition. Our MD simulation (discussed in the following) also shows the

Nanoscale

а 5.5 s 10.5 s b d C Fast Size Growth Slow Growth and Stabilization Liposome 100 90 80 70 Liposome Liposome size (D, nm) 60 50 40 30 20 10 8 10 12 14 Time (s) е

Fig. 2 Growth of PC liposomes visualized in real-time by GLC-TEM. (a) Time-lapse TEM images of the liposomes evolution. (b) The corresponding size growth plot for the evolution of a PC liposome during the first 15 s from an aqueous solution of phosphatidylcholine lipids. (c) and (d) TEM images taken from liquid solution indicating the coexistence of the small micelle-like structures and liposomes. (e) Schematic illustration of mechanism of the PC liposome evolution. TEM images are taken from Video S1.† The scale bar is 20 nm.

Growing liposome

Forming lipid aggregates

(micelle-like structures)

PC lipid molecule

Forming liposome

Mature liposome

formation of such aggregates or micelle-like structures and their transformation to liposome. Overall, by considering these facts and knowing that micelle-like structures should have at least 2-3 nm size to be detectable by liquid-cell TEM, we believe that liposome formation is followed by lipids aggregates or micelle-like structures.

Kinetics of the liposome growth is also shown in Fig. 2b. As it can be seen, the initial growth of the liposomes is very fast (10-15 nm s⁻¹) which can be attributed to the coalescence of the lipid aggregates resembling micelle-like structures. A relatively slow growth of liposomes (2-5 nm s⁻¹) during the second stage of the liposome evolution (Fig. 2b) can be correlated to the rearrangement of the diffusing lipids within the self-assembled structures. This indicates that the assemblies continue to grow as the neighboring lipid molecules diffuse into the self-assembled structures (Fig. 2b). Eventually, stable liposomes are observed (third stage in Fig. 2b) as the lipids within the bulk solution are depleted. There also exist a critical membrane size at which vesiculation is energetically unfavored below that size.⁶² This supports our observation of stable PC liposome showing size ranges between 50-200 nm. A similar behavior for the evolution of PC liposomes from a different liquid pocket is also shown in Fig. S4† (Video S2†). The results confirm three distinct stages for the liposomal growth namely fast initial growth, slow continued growth, and liposome stabilization can be clearly identified. The original TEM images given in Fig. S4† are shown in Fig. S5.† The shape and size of the PC liposomes that are self-assembled in the aqueous phase within GLC are also analogous to that prepared ex situ and analyzed by cryo-TEM (Fig. S6†) and scanning electron microscopy (SEM) (Fig. S7†).

Note that measured thickness of liposome membranes matches the expected values. The membrane thickness of the liposomes is measured to be approximately 4.3 nm as shown in Fig. S8.† Note that the length of an induvial PC lipid is approximately 2 nm. This thickness is similar to the membrane thickness of PC liposomes reported in the literature. 60,61 Furthermore, our MD simulation result (Fig. 3) for the membrane size matches well with the experimentally measured thickness values.

We believe the presence of cholesterol and salts in PBS facilitate the contrast for TEM imaging and keeping the liposomes stable under electron beam radiation. As it is shown in Fig. S9,† PC liposomes with cholesterol in pure water (no salt) exhibit much less image contrast compared to the PC liposomes in the presence of salt. The effect of salt molecules can be correlated to the compact packing of the polar segments of the lipids in the bilayer membrane which is also reported elsewhere. 2,63-65 Moreover, the cholesterol molecules also are known to contribute to the compact packing of the nonpolar

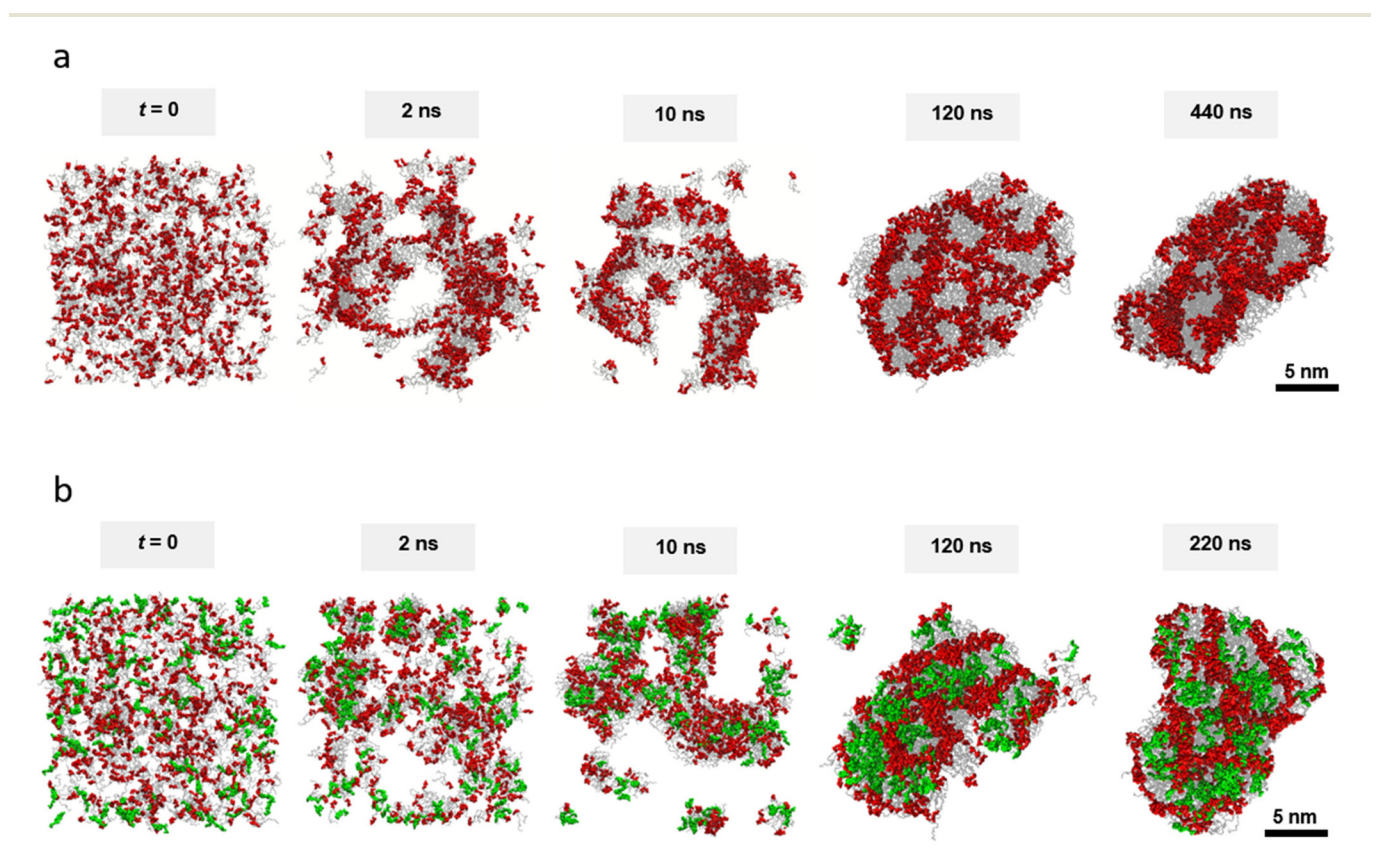


Fig. 3 MD simulations of phosphatidylcholine self-assembly. (a) Simulation snapshots of 512 PC molecules in aqueous solution in a 19 nm periodic box. These images are taken from Video S3.† (b) Analogous PC system in the presence of 128 cholesterol molecules. These images are taken from Video S4.† Red = zwitterionic PC fragments; Grey = hydrophobic PC fragments; Green = cholesterol molecules.

segments of the lipid molecules, leading to a more stable liposomal structure.^{66–70} This can be clearly seen from the deformed and denatured liposomes formed in the absence of the cholesterol molecules (Fig. S10†).

Nanoscale

To better understand the process phosphatidylcholine self-assembly and reorganization, we carried out the molecular dynamics (MD) simulations of PC molecules in 140 mM aqueous salt solutions with and without the presence of cholesterol. Fig. 3 shows that within several nanoseconds PC coalesce in both systems into small clusters since PC molecules are present in oversaturated concentrations in water (CMC). Fig. 3a reveals that these random clusters further aggregate into mesh-like structures of randomly stacked pieces of double-layer membranes. This process is driven by the separate attraction of zwitterionic hydrophilic fragments and hydrophobic chains in PCs, each of which assemble into bilayer structures. Subsequently, the aggregates slowly reorganize into larger phospholipid bilayers that produce cheese-like three-dimensional patterns.

In Fig. 3b, we can see that cholesterol become entrapped within hydrophobic regions of the assemblies. These regions

become wider, with less zwitterionic bridges between the polar exterior, so the system can have reduced surface tensions and increased stability. These stacked membrane fragments are assumed to merge, trap water and reorganize into proto-liposomes. These proto-liposomes grow by sucking water and reorganize into thermodynamically stable liposomes, once the loose PCs disappear from their membranes.

The fusion of PC liposomes through lipid bilayer membranes are monitored and visualized in real-time by GLC-TEM, as shown in Fig. 4a (Video S5†). Blue and green arrows indicate the two different liposomes which are growing and come to contact with each other. Orange arrows indicate the evolution of interface between the two PC liposomes. Exploring lipid fusion in liposomal systems can offer a useful approach to understand the complex process of membrane fusion in biological systems.⁷² The fusion process of biological membranes is suggested to be a rapid, efficient, and controlled process.^{72,73} The biomembranes fusion combined with controlled release of encapsulated content is vital for cell signaling, exocytosis, endocytosis, and intracellular trafficking. As shown in Fig. 4b, we observe cellular membrane fusion to

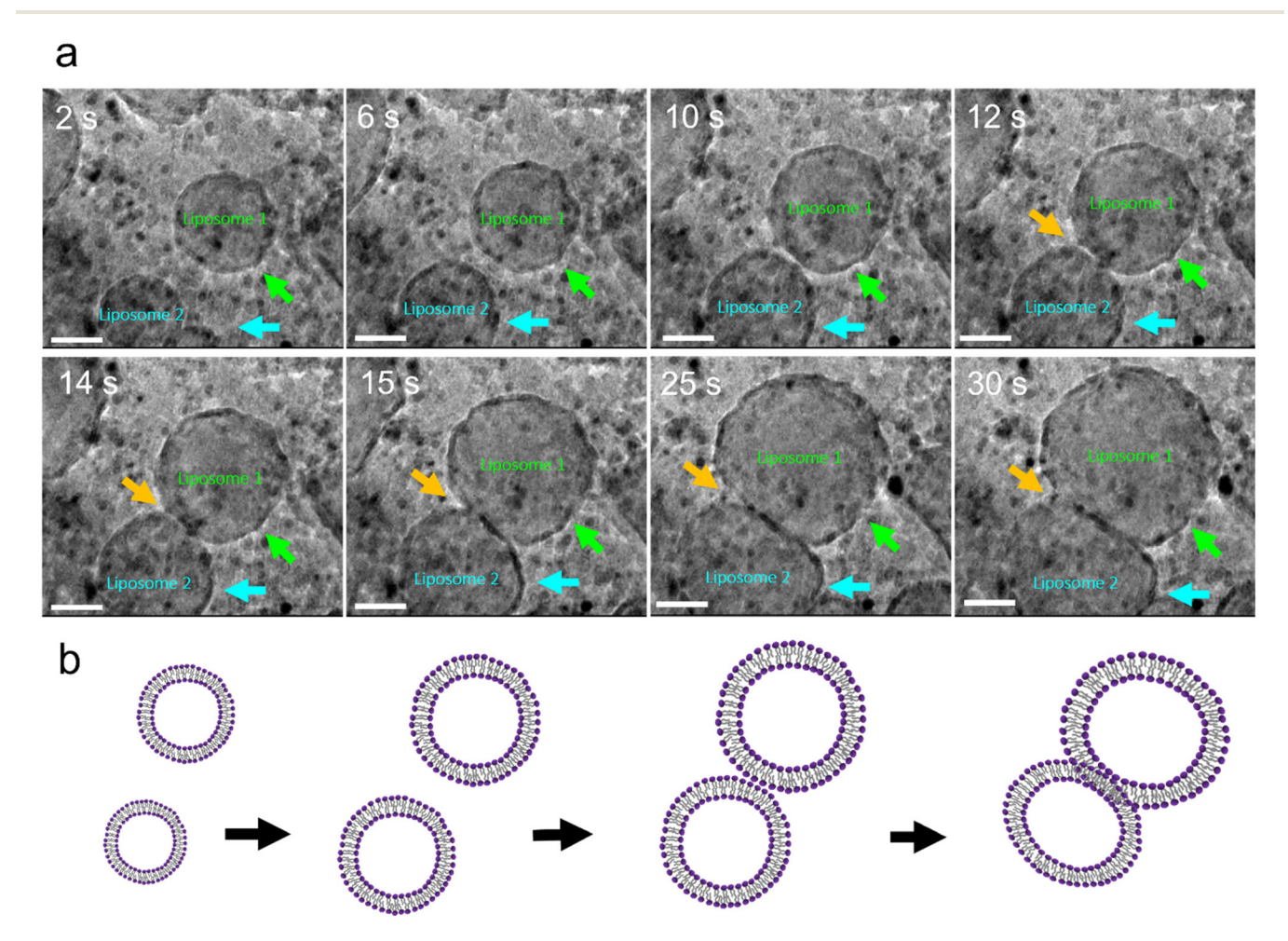


Fig. 4 Fusion of PC liposomes visualized in real-time by GLC-TEM. (a) Time-lapsed fusion of two PC liposomes in real-time. Scale bar is 20 nm. TEM images are taken from Video S5.† (b) Schematic illustration of proposed mechanism of the liposomal fusion.

proceed in three stages: intermediate stage of apposed lipid bilayers docking, coalescence of proximal leaflets and formation of a hemifusion diaphragm, and the fusion pore opening. This is analogous to the cryo-TEM results reported in the literature at which liposomes docking and hemifusion are identified as intermediate states. 62 We also observe that docked large PC liposomes (Fig. S11†) show a longer lifetime than the docked small PC liposomes which can be ascribed to decreased curvature stress of large liposomes. A full fusion of two adjacent liposomes after a hemifusion can be seen in Video S6.†

Our liposome fusion results verifies the models proposed for the fusion of liposomes and vesicles. 1,2,20,74 The understanding of phase behavior of lipid mixtures combined with studying intermediate non-bilayer structures during lipid bilayers fusion can help to control non-bilayer lipid phases and lipid bilayers fusion. In the absence of any membranedeforming or -destabilizing mechanism, membrane fusion will be dependent on the likelihood of spontaneous fusion (as observed in this study). In a recent work by François-Martin et al. 75 it is shown that spontaneous membrane fusion occur between liposomes made of phosphocholine lipids at a relatively low energy barrier. If two membranes are in a proximity of each other, the spontaneous fusion probability can increase due to the higher frequency of Brownian collisions between the lipid bilayers.

Due to thermodynamic and strain-induced instability, liposomes have tendency to denature and breakdown into the constituting lipids. Liposomes degradation is shown to occur as result of structural instability and deformation of the lipid bilayer membrane, followed by rupture and disintegration of the lipid membrane. 62 Self-denaturation can be mainly described as consequence of instability caused by local dilution of lipids and strain. It is known that liposome breakdown involves significant permeability change caused by transient pores formed by packing distortions, followed by a lysis and rupture of the lipid bilayer assemblies. 76 This is demonstrated by the release of a fluorescent agent encapsulated into liposomes.76 Although the degradation and denaturation of liposomes is well-known, yet there is no direct, real-time observation of these processes. Thus, the real-time visualization of liposomes self-disintegration herein can also examine the details of the established theories. Fig. 5a (Video S7†) shows time-lapse series of the denaturation of a PC liposome in realtime. A schematic illustration of the PC liposome disintegration is also shown in Fig. 5b. Consistent with the previously reported literature, the liposome denaturation is a spontaneous process at which a self-assembled structure (liposome) breaks down into the constituting molecules (lipids). Fig. S12 and S13† also illustrate breakdown of smaller PC liposomes and their coalescence with the adjacent larger PC liposomes.

In addition to triggering the formation of liposomes, other beam effects should be taken into account. These are shown in Fig. S14† for different types of electron beam-induced effects on liquid cell-TEM studies. One important aspect can be the change in the local pH of the solution. 52,55,77,78 Indeed, membrane lipids are directly influenced by solution pH, due to lipids acido-basic properties, and pH change could induce migration and deformation.^{77,78} vesicles lipids-based Formation of bubbles using high electron doses have been previously reported. 52,55 Displacement of liquid fluid by generated gas is an undesired effect in liquid cell-TEM experiments

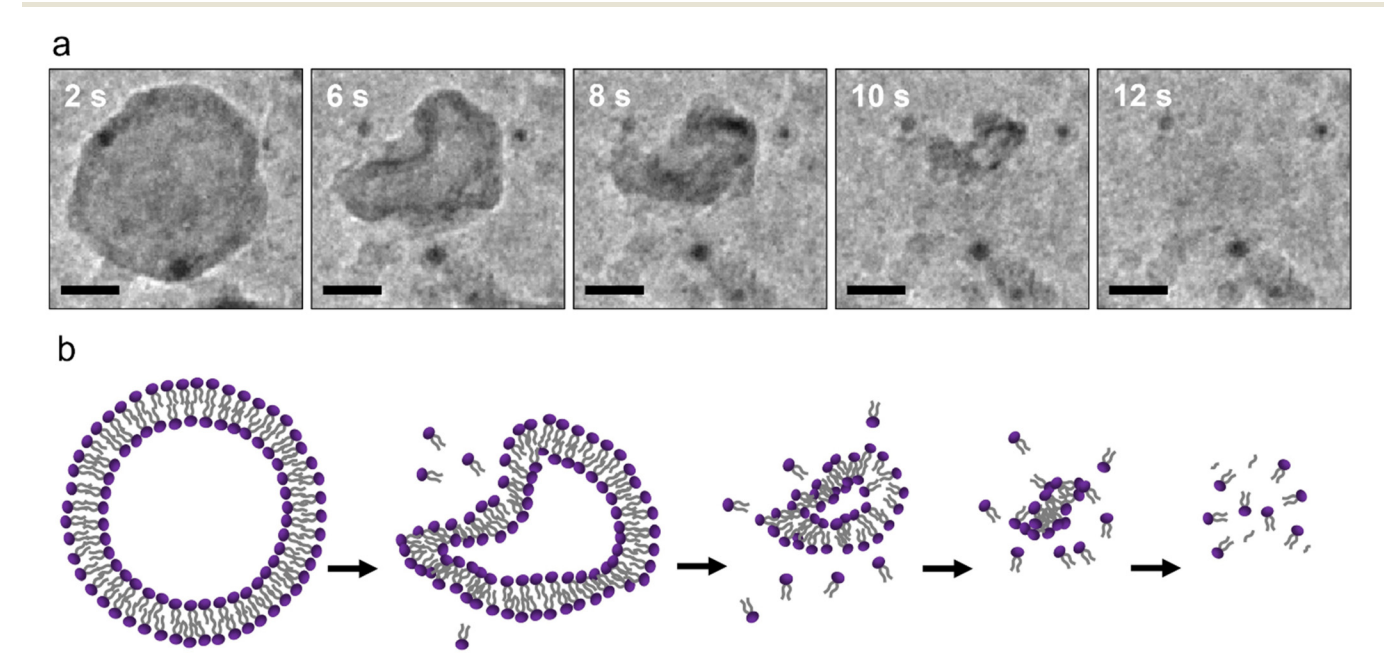


Fig. 5 Denaturation of PC liposomes visualized in real-time by GLC-TEM. (a) Time-lapse TEM images of denaturation (breakdown) of a PC liposome, visualized in real-time by GLC-TEM. Scale bar is 10 nm. TEM images are taken from Video S7.† (b) Schematic illustration of proposed mechanism of the PC liposome denaturation.

Nanoscale Paper

which are correlated to high electron doses. 52,55 For instance, self-denaturation (caused by the local lipids dilution and shape strain mechanism) is also a common natural phenomenon in liposomes. Therefore, liposomes degradation can be correlated to the self-denaturation or electron beam effect.

We believe that the low electron dose used in this study significantly minimizes such effect during the TEM imaging.⁵⁵ To minimize the electron beam effect on liposomes (e.g., liposome breakdown, pH change, bubble formation), we have chosen a relatively low electron dose rate (~1.9 e A⁻² s⁻¹). As can be seen from Fig. S12 and S13,† while one liposome starts to breakdown into the composing phospholipids, the surrounding liposomes retain their integrity throughout the exposure to electron beam. Thus, liposomes rupture and breakdown can be mainly ascribed to self-denaturation rather than electron beam-induced degradation.

During in situ liquid phase-TEM imaging of liposomes, we also noticed an interesting phenomenon which involves both denaturation and fusion of small proximate liposomes (Fig. 6 and Video S8†). It can be seen that some liposomes denature and the constituting lipids integrate into the adjacent liposome, resulting in rearrangement of the host lipid bilayer membrane and growth of the lipids-receiving liposome. This event occurs for several PC liposomes periodically and eventually the last small liposome denatures and integrate its constituting lipids into a large liposome. It is important to note that large PC liposomes show more stability towards denaturation compared to the small PC liposomes, which can be correlated to the reduced strain of the large liposome. 13,72,76 This can explain why liposomes have natural tendency to fuse and grow.

Also note should be given to the presence of water during imaging and reasons behind the high contrast of imaged liposomes. The high contrast images can be attributed to the presence of salt in the solution as well as thin liquid encapsulated between ultrathin graphene layers. As it was also discussed in the manuscript, PC liposomes in the absence of salt (Fig. S9†) exhibit much less contrast compared to the PC liposomes in the presence of salt. The effect of salt molecules can be correlated to the compact packing of the polar segments of the

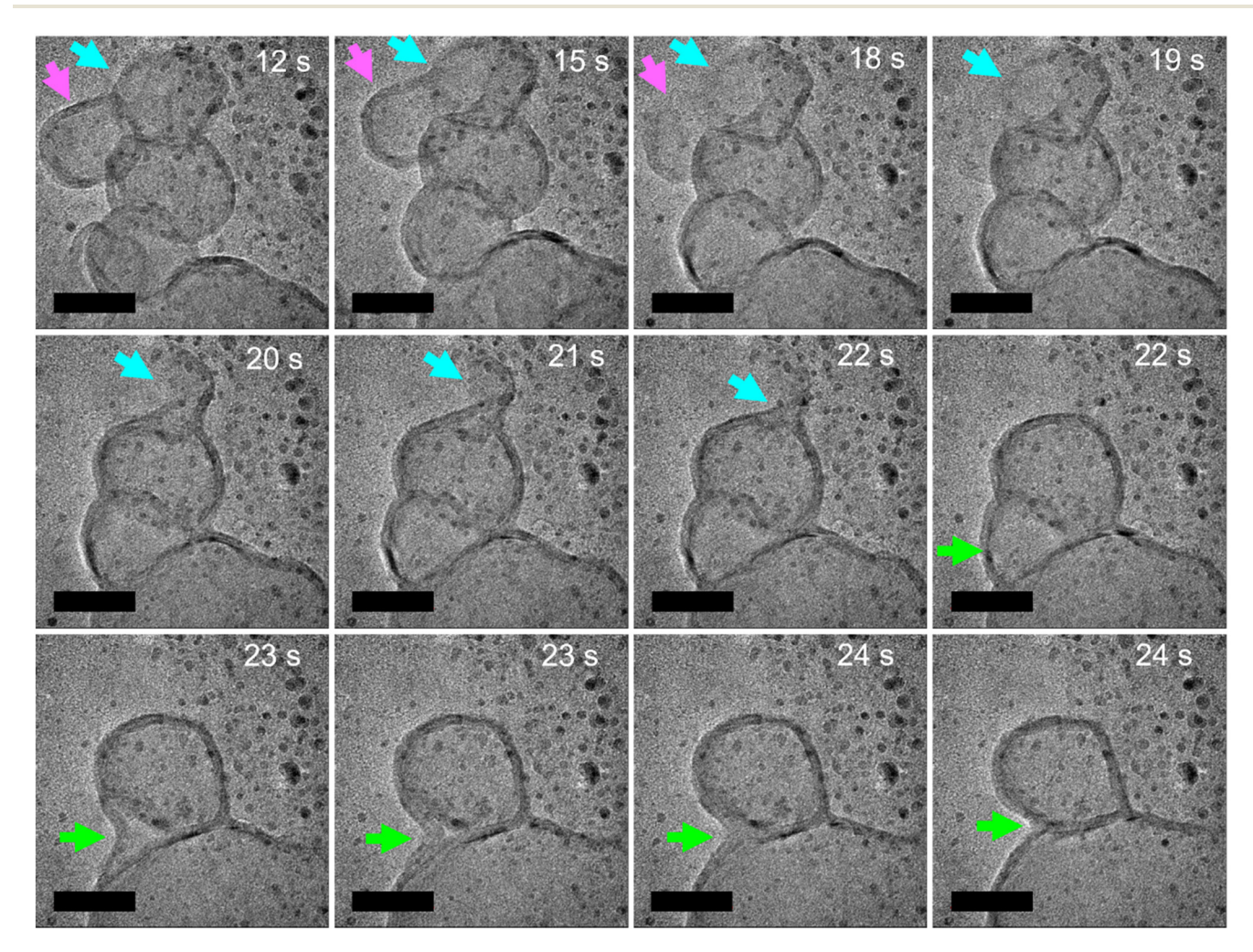


Fig. 6 Time-lapse TEM images of simultaneously occurring fusion and denaturation (breakdown) of a liposomal aggregate in real-time. Green, blue, and pink arrows point out different denaturing PC liposomes. Scale bar is 50 nm. The TEM images are taken from Video S8.†

lipids in the bilayer membrane which is also reported elsewhere. 2,63-65 Furthermore, the enhanced contrast can be ascribed to thin liquid layer encapsulated between graphene layers. This can be contrasted by a relatively poor spatial resolution of liposomes in SiNx liquid cell-TEM due to thick SiN_r membranes and thick solvent layer.³ Moreover, our videos show fast and very mobile movements of the lipids-based structures. A dried liquid cell indeed lacks such facile and fast dynamics of liposomes. This can be seen in Video S9† as result of transformation of a wet liquid cell (with a dark contrast and mobile small micelle-like structures) into a dry liquid cell (with a colorless or white contrast and still micelle-like structures). The presence of water in a liquid cell can also be verified by electron energy loss spectroscopy (EELS)36,79-81 to measure water exciton or oxygen, bubble formation, 79,81 and liquid thickness measurement. 79,81 We have monitored the presence of water in GLC during the TEM imaging by EELS as shown in Fig. S15.† Low loss EELS data exhibit a peak ~7 eV related to the water optical gap, a peak ~9 eV related to water exciton peak, and a peak ~14 eV related to graphene $\sigma + \pi$ bond. This further indicates the presence of water (wet GLC) during TEM imaging. The formation of bubbles due to electron beam-induced radiolysis further confirm the presence of water in the GLC. The presence of bubbles as shown in Video S10† further indicates the presence of water in the GLC. Indeed, bubbles have very distinct contrast (white or colorless) compared to the surrounding liquid area (dark).

In summary, we demonstrate some of the fundamental stages, including formation and growth, fusion, and denaturation of liposomes made of phosphatidylcholine as a model lipid. This study offers new insights on formation and evolution of liposomes in hydrated environment, which can be used toward further understanding of biological membranes and developing liposome-based drug delivery systems.

Conclusion

In this study, the evolution of PC liposomes via self-assembly of phosphatidylcholine are visualized in real-time by GLC-TEM. The formation of PC liposomes is initiated by lipids aggregates resembling micelle-like structures. These small assemblies evolve by coalescence resulting in fast growth of liposomes. This is followed by slow growth of liposomes as lipid molecules diffuse into the assembled structures. The growth slows down as the result of lipid consumption and rearrangement within the assembled structures, and eventually leading to stable liposomes. These findings are further confirmed by molecular dynamics (MD) simulation. Fusion of PC liposomes is also found to proceed as intermediate stage of apposed lipid bilayers docking, coalescence of proximal leaflets and formation of a hemifusion diaphragm, and the fusion pore opening. Denaturation of PC liposomes is described as the result of structural instability and deformation of the lipid bilayer membrane, followed by rupture and disintegration of the lipid membrane. This study offers new insights on fundamental steps concerning liposomes evolution for different applications, for example, drug delivery systems, and behavior of biological membranes in aqueous environment, among others

Author contributions

This study is conceptualized by V. J. and R. S.-Y.; V. J. conducted the liposome synthesis and electron microscopy experiments. M. S. and P. K. performed the MD simulations. A. A. made major contributions by careful analysis of TEM videos and the quantification of TEM images, and EELS data acquisition. She also contributed on the preparation of figures and schematics. V. J. led the writing of the manuscript and all co-authors contributed to the revision of the manuscript, preparation of figures, and ESI.†

Conflicts of interest

There are no conflicts to declare.

Acknowledgements

R. Shahbazian-Yassar acknowledges the financial support from the National Science Foundation (NSF) award number DMR-1809439. Authors also acknowledge the Research Resources Center (RRC) at the University of Illinois at Chicago (UIC) especially Director of Electron Microscopy Core, Dr Fengyuan Shi.

References

- 1 X. Q. Wei, J. F. Zhu, X. B. Wang and K. Ba, ACS Omega, 2020, 5, 1120-1126.
- 2 K. Gnanasekaran, H. Chang, P. J. M. Smeets, J. Korpanty, F. M. Geiger and N. C. Gianneschi, Nano Lett., 2020, 20, 4292-4297.
- 3 S. M. Hoppe, D. Y. Sasaki, A. N. Kinghorn and K. Hattar, Langmuir, 2013, 29, 9958-9961.
- 4 Y. P. Patil and S. Jadhav, Chem. Phys. Lipids, 2014, 177, 8-
- 5 L. Maja, K. Željko and P. Mateja, J. Supercrit. Fluids, 2020, 165, 1-17.
- 6 G. Liu, S. Hou, P. Tong and J. Li, Crit. Rev. Anal. Chem., 2022, 52, 392-412.
- 7 A. Akbarzadeh, R. Rezaei-Sadabady, S. Davaran, S. W. Joo, N. Zarghami, Y. Hanifehpour, M. Samiei, M. Kouhi and K. Nejati-Koshki, Nanoscale Res. Lett., 2013, 8, 1.
- 8 M. A. Touve, D. B. Wright, C. Mu, H. Sun, C. Park and N. C. Gianneschi, Macromolecules, 2019, 52, 5529-5537.
- 9 M. A. Touve, C. A. Figg, D. B. Wright, C. Park, J. Cantlon, B. S. Sumerlin and N. C. Gianneschi, ACS Cent. Sci., 2018, 4, 543-547.

10 R. Tenchov, R. Bird, A. E. Curtze and Q. Zhou, ACS Nano, 2021, 15, 16982-17015.

Nanoscale

- 11 K. Soo, X. Sun, M. E. Aikins and J. J. Moon, Adv. Drug Delivery Rev., 2021, 169, 137-151.
- 12 R. Vartak, S. M. Patil, A. Saraswat, M. Patki, N. K. Kunda and K. Patel, Nanomedicine, 2021, 16, 1187-1202.
- 13 S. Sandin, D. Gravano, C. Randolph, M. Sharma and E. de Alba, Pharmaceutics, 2021, 13, 583.
- 14 C. B. Fox, S. K. Mulligan, J. Sung, Q. M. Dowling, H. W. M. Fung, T. S. Vedvick and R. N. Coler, Int. J. Nanomed., 2014, 9, 1367-1377.
- 15 M. Rasoulianboroujeni, G. Kupgan, F. Moghadam, M. Tahriri, A. Boughdachi, P. Khoshkenar, J. J. Ambrose, N. Kiaie, D. Vashaee, J. D. Ramsey and L. Tayebi, Mater. Sci. Eng., C, 2017, 75, 191-197.
- 16 C. Faure, A. Derré and W. Neri, J. Phys. Chem. B, 2003, 107, 4738-4746.
- 17 M. E. Meyre, O. Lambert, B. Desbat and C. Faure, Nanotechnology, 2006, 17, 1193-1201.
- 18 D. Marsh, Biophys. J., 2012, 102, 1079-1087.
- 19 J. Kotouček, F. Hubatka, J. Mašek, P. Kulich, K. Velínská, J. Bezděková, M. Fojtíková, E. Bartheldyová, A. Tomečková, J. Stráská, D. Hrebík, S. Macaulay, I. Kratochvílová, M. Raška and J. Turánek, Sci. Rep., 2020, 10, 1-11.
- 20 J. M. Hernandez, A. Stein, E. Behrmann, D. Riedel, A. Cypionka, Z. Farsi, P. J. Walla, S. Raunser and R. Jahn, Science, 2012, 336, 1581-1584.
- 21 J. P. Patterson, P. Abellan, M. S. Denny, C. Park, N. D. Browning, S. M. Cohen, J. E. Evans and N. C. Gianneschi, J. Am. Chem. Soc., 2015, 137, 7322–7328.
- 22 C. Li, C. C. Tho, D. Galaktionova, X. Chen, P. Král and U. Mirsaidov, Nanoscale, 2019, 11, 2299-2305.
- 23 K. H. Nagamanasa, H. Wang and S. Granick, Adv. Mater., 2017, 29, 1-6.
- 24 A. Bremer, C. Henn, A. Engel, W. Baumeister and U. Aebi, *Ultramicroscopy*, 1992, **46**, 85–111.
- 25 H. Friedrich, P. M. Frederik, G. De With and N. A. J. M. Sommerdijk, Angew. Chem., Int. Ed., 2010, 49, 7850-7858.
- 26 R. Van Zanten and J. A. Zasadzinski, Curr. Opin. Colloid Interface Sci., 2005, 10, 261-268.
- 27 B. J. Smith, L. R. Parent, A. C. Overholts, P. A. Beaucage, R. P. Bisbey, A. D. Chavez, N. Hwang, C. Park, A. M. Evans, N. C. Gianneschi and W. R. Dichtel, ACS Cent. Sci., 2017, 3, 58-65.
- 28 D. L. Anderson, New Theory Earth, 2012, pp. 356-374.
- 29 I. N. Dahmke, A. Verch, J. Hermannsdörfer, D. B. Peckys, R. S. Weatherup, S. Hofmann and N. De Jonge, ACS Nano, 2017, 11, 11108-11117.
- 30 M. Textor and N. De Jonge, Nano Lett., 2018, 18, 3313-
- 31 H. Cho, M. R. Jones, S. C. Nguyen, M. R. Hauwiller, A. Zettl and A. P. Alivisatos, Nano Lett., 2017, 17, 414-420.
- 32 D. J. Kelly, M. Zhou, N. Clark, M. J. Hamer, E. A. Lewis, A. M. Rakowski, S. J. Haigh and R. V. Gorbachev, Nano Lett., 2018, 18, 1168-1174.

- 33 Q. Chen, J. M. Smith, J. Park, K. Kim, D. Ho, H. I. Rasool, A. Zettl and A. P. Alivisatos, Nano Lett., 2013, 13, 4556-
- 34 E. Firlar, M. Ouy, A. Bogdanowicz, L. Covnot, B. Song, Y. Nadkarni, R. Shahbazian-Yassar and T. Shokuhfar, Nanoscale, 2019, 11, 698-705.
- 35 S. Narayanan, R. Shahbazian-Yassar and T. Shokuhfar, ACS Biomater. Sci. Eng., 2020, 6, 3208-3216.
- 36 E. Firlar, M. Ouy, L. Covnot, Y. Xing, D. Lee, A. Chan, Y. He, B. Song, S. Afelik, Y. Wang, R. Shahbazian-Yassar, J. Oberholzer and T. Shokuhfar, Int. J. Nanomed., 2019, 14, 371-382.
- 37 S. Narayanan, E. Firlar, M. G. Rasul, T. Foroozan, N. Farajpour, L. Covnot, R. Shahbazian-Yassar and T. Shokuhfar, Nanoscale, 2019, 11, 16868-16878.
- 38 S. Keskin, S. Besztejan, G. Kassier, S. Manz, R. Bücker, S. Riekeberg, H. K. Trieu, A. Rentmeister and R. J. D. Miller, J. Phys. Chem. Lett., 2015, 6, 4487-4492.
- 39 J. C. Phillips, K. Schulten, A. Bhatele, C. Mei, Y. Sun, E. J. Bohm and L. V. Kale, Parallel Sci. Eng. Appl. Charm++ Approach, 2016, vol. 26, pp. 60-76.
- 40 K. Vanommeslaeghe, E. Hatcher, C. Acharya, S. Kundu, S. Zhong, J. Shim, E. Darian, O. Guvench, P. Lopes, I. Vorobyov and A. D. MacKerell Jr., J. Comput. Chem., 2010, 31,671-690.
- 41 R. Shediac and T. Raphael, J. Comput. Chem., 2012, 33, 2451-2468.
- 42 T. Darden, D. York and L. Pedersen, J. Chem. Phys., 1993, 98, 10089-10092.
- 43 C. Huang, D. Quinn, Y. Sadovsky, S. Suresh and K. J. Hsia, Proc. Natl. Acad. Sci. U. S. A., 2017, 114, 2910-2915.
- 44 M. C. A. Stuart and E. J. Boekema, Biochim. Biophys. Acta, Biomembr., 2007, 1768, 2681-2689.
- 45 S. Mondal, A. Pan, S. Das, S. P. Moulik and S. Ghosh, RSC Adv., 2016, 6, 26019-26025.
- 46 H. Nakanishi, K. Tsuchiya, T. Ohkubo, H. Sakai and M. Abe, J. Oleo Sci., 2005, 54, 443-451.
- 47 M. Cano-Sarabia, A. Angelova, N. Ventosa, S. Lesieur and J. Veciana, J. Colloid Interface Sci., 2010, 350, 10-15.
- 48 I. A. Chen and J. W. Szostak, Biophys. J., 2004, 87, 988-
- 49 B. Fritsch, A. Hutzler, M. Wu, S. Khadivianazar, L. Vogl, M. P. M. Jank, M. März and E. Spiecker, Nanoscale Adv., 2021, 3, 2466-2474.
- 50 T. H. Hsieh, J. Y. Chen, C. W. Huang and W. W. Wu, Chem. Mater., 2016, 28, 4507-4511.
- 51 J. M. Zook and W. N. Vreeland, Soft Matter, 2010, 6, 1352-
- 52 N. M. Schneider, M. M. Norton, B. J. Mendel, J. M. Grogan, F. M. Ross and H. H. Bau, J. Phys. Chem. C, 2014, 118, 22373-22382.
- 53 S. Pu, C. Gong and A. W. Robertson, R. Soc. Open Sci., 2019, 7, 191204.
- 54 N. D. Loh, S. Sen, M. Bosman, S. F. Tan, J. Zhong, C. A. Nijhuis, P. Král, P. Matsudaira and U. Mirsaidov, Nat. Chem., 2017, 9, 77-82.

Paper

55 P. Abellan, T. J. Woehl, L. R. Parent, N. D. Browning, J. E. Evans and I. Arslan, Chem. Commun., 2014, 50, 4873-

- 56 K. Slimani, L. Moine, C. Aymes-Chodur, A. Laurent, D. Labarre and N. Yagoubi, Polym. Degrad. Stab., 2009, 94, 584-590.
- 57 T. Ito, W. Yamada, L. Zhou, F. Amita and O. Kajimoto, IAERI, 2000, 239-242.
- 58 D. Li, M. Nielsen, J. Lee, C. Frandsen, J. Banfield and J. J. De Yoreo, Science, 2012, 336, 1014-1018.
- 59 J. M. Grogan, L. Rotkina and H. H. Bau, Phys. Rev. E: Stat., Nonlinear, Soft Matter Phys., 2011, 83, 1-5.
- 60 T. H. Lee, M. A. Sani, S. Overall, F. Separovic and M. I. Aguilar, Biochim. Biophys. Acta, Biomembr., 2018, 1860, 300-309.
- 61 C. M. Cooke, H. Moloo, M. W. H. Suen and S. S. Singh, J. Endometr. Pelvic Pain Disord., 2018, 10, 124-128.
- 62 C. M. Lin, G. P. Chang, H. K. Tsao and Y. J. Sheng, J. Chem. Phys., 2011, 135, 045102.
- 63 F. R. Lin, J. K. Niparko and L. Ferrucci, Bone, 2014, 23, 1-7.
- 64 H. I. Petrache, S. Tristram-Nagle, D. Harries, N. Kuĉerka, J. F. Nagle and V. A. Parsegian, J. Lipid Res., 2006, 47, 302-309.
- 65 J. U. De Mel, S. Gupta, R. M. Perera, L. Ngo, P. Zolnierczuk, M. Bleuel, S. V. Pingali and G. J. Schneider, Langmuir, 2020, **36**, 9356-9367.
- 66 S. A. Pandit, D. Bostick and M. L. Berkowitz, Biophys. J., 2004, 86, 1345-1356.
- 67 S. W. Chiu, E. Jakobsson, R. J. Mashl and H. L. Scott, Biophys. J., 2002, 83, 1842-1853.
- 68 C. Hofsäß, E. Lindahl and O. Edholm, Biophys. J., 2003, 84, 2192-2206.

- 69 P. Nakhaei, R. Margiana, D. O. Bokov, W. K. Abdelbasset, M. A. J. Kouhbanani, R. S. Varma, F. Marofi, M. Jarahian and N. Beheshtkhoo, Front. Bioeng. Biotechnol., 2021, 9, 1-23.
- 70 K. Tu, M. L. Klein and D. J. Tobias, Biophys. J., 1998, 75, 2147-2156.
- 71 S. Sen, Y. Han, P. Rehak, L. Vuković and P. Král, Chem. Soc. Rev., 2018, 47, 3849-3860.
- 72 O. Ries, P. M. G. Löffler, A. Rabe, J. J. Malavan and S. Vogel, Org. Biomol. Chem., 2017, 15, 8936-8945.
- 73 M. Hu, F. Stanzione, A. K. Sum, R. Faller and M. Deserno, ACS Nano, 2015, 9, 9942-9954.
- 74 R. Gharib, H. Greige-Gerges, S. Fourmentin, C. Charcosset and L. Auezova, Carbohydr. Polym., 2015, 129, 175-186.
- 75 C. François-Martin, J. E. Rothman and F. Pincet, Proc. Natl. Acad. Sci. U. S. A., 2017, 114, 1238-1241.
- 76 A. Domecq, E. A. Disalvo, D. L. Bernik, F. Florenzano and M. J. Politi, Drug Deliv. J. Deliv. Target. Ther. Agents, 2001, 8, 155-160.
- 77 A. Zidovska, K. K. Ewert, J. Quispe, B. Carragher, C. S. Potter and C. R. Safinya, Biochim. Biophys. Acta, Biomembr., 2009, 1788, 1869-1876.
- 78 M. I. Angelova, A. F. Bitbol, M. Seigneuret, G. Staneva, A. Kodama, Y. Sakuma, T. Kawakatsu, M. Imai and N. Puff, Biochim. Biophys. Acta, Biomembr., 2018, 1860, 2042-2063.
- Ghodsi, S. Anand, R. Shahbazian-Yassar, 79 S. T. Shokuhfar and C. M. Megaridis, ACS Nano, 2019, 13, 4677-4685.
- 80 S. Information.
- 81 S. Keskin, C. Pawell and N. de Jonge, Micron, 2021, 149, 103109.